

Article

Simulation Analysis of Acoustic Radiation from Force Excitation of Foam-Filled Stiffened Sandwich Panels

Bin Li ^{*}, Ning Wang, Haoyang Ding, Zilai Zheng, Wenjian Kuang and Langlang Wei

School of Mechanical Engineering, Wuhan Polytechnic University, Wuhan 430023, China; wangning20000525@163.com (N.W.); d20200512018@163.com (H.D.); wldxt@foxmail.com (Z.Z.); jaden1999@163.com (W.K.); 13871944204@163.com (L.W.)

* Correspondence: lb420@whpu.edu.cn

Abstract: To tackle the influence of foam filling on the sound radiation performance of reinforced sandwich panels, this study employs a combined approach of experiments and simulations to investigate the factors that impact the sound radiation performance in the 1–2000 Hz mid–low frequency range. The aim is to determine how the parameters of foam impact the sound radiation performance of foam-filled reinforced sandwich panels. The results indicate that changes in the acoustic parameters of the foam have a weak effect on the frequency corresponding to the peak sound radiation power and the non-peak frequency range sound radiation performance of the sandwich panel, while significantly impacting the peak sound radiation power. Among them, porosity has the least influence on sound radiation performance, whereas static flow resistivity and tortuosity factors have a greater influence on peak sound radiation performance. The reduction in thermal characteristic length and the increase in static flow resistivity can both enhance the sound radiation performance of the panel, while the impact of tortuosity factor and viscous characteristic length on panel sound radiation performance depends on the frequency range.

Keywords: foam-filled; reinforced laminated plate; sound radiation



Citation: Li, B.; Wang, N.; Ding, H.; Zheng, Z.; Kuang, W.; Wei, L. Simulation Analysis of Acoustic Radiation from Force Excitation of Foam-Filled Stiffened Sandwich Panels. *Appl. Sci.* **2023**, *13*, 10733. <https://doi.org/10.3390/app131910733>

Academic Editors: Claudio Guarnaccia and Domenico Rossi

Received: 2 September 2023
Revised: 21 September 2023
Accepted: 25 September 2023
Published: 27 September 2023



Copyright: © 2023 by the authors. Licensee MDPI, Basel, Switzerland. This article is an open access article distributed under the terms and conditions of the Creative Commons Attribution (CC BY) license (<https://creativecommons.org/licenses/by/4.0/>).

1. Introduction

Noise issues are widely present in both living and working environments and are now considered the second largest environmental concern after air pollution [1]. The sound radiation resulting from mechanical vibrations can cause physical and psychological harm to users or people in proximity and can also impact the functionality of the machinery itself, for example, the stealth capability of submarines or the effectiveness of sonar systems [2,3]. Reinforced double-layer panel structures, as a basic type of structure, are widely used in various fields such as vehicles, ships, aviation, agriculture, construction, and defense. These panels offer better sound and vibration performance than plate structures with the same volume or weight. Additionally, they decrease sound radiation effectively if the internally reinforced cavity is filled with foam. Its advantages include high strength, high rigidity, light weight, excellent damping performance, energy absorption performance, sound insulation performance, thermal insulation performance, etc. [4–6]. However, it has a relatively high manufacturing cost, and several factors need to be considered during the design and manufacturing process [7]. As a result, the sound control concerns of foam-filled reinforced sandwich panel structures are gaining greater attention and are of great research importance.

Advanced sandwich panels come in various types, including polyurethane core, mineral wool core, and polystyrene core [8]. Currently, Thamburaj et al. [9] conducted theoretical analysis and finite element simulations to investigate the optimization of anisotropic sandwich beams. They found that parameters such as the thickness, density, and elastic modulus of anisotropic cores significantly impact sound transmission performance.

Through optimization design, they achieved maximum transmission loss within a specified frequency range. Wang [10] examined the acoustic and vibration characteristics of sandwich panel structures with a wood core and polyurethane foam filling by means of numerical research and simulation analysis in his master's thesis. The findings suggest that the panels filled with polyurethane foam demonstrated excellent sound insulation capabilities. Arunkumar et al. [11] performed a simulation analysis exploring the effects of polyurethane foam filling on the acoustic and vibration characteristics of truss sandwich panels. The results of the study indicated that this approach reduced the resonance amplitudes of both vibration and acoustic responses significantly. Khan et al. [12] provided an overview of basic polyurethane foam core structures, advanced polyurethane foam core composite materials with various reinforcing materials, and complex structures such as hybrid core panels. In recent years, these have found extensive applications and commercial prospects in fields such as mechanics, electrical engineering, dynamics, thermodynamics, and acoustics. Li et al. [13] carried out both theoretical and experimental investigations on the acoustic and vibration properties of fiber-reinforced polymer laminates featuring porous foam cores when subjected to planar acoustic excitation. Zengquan Zheng et al. [14] conducted a series of simulation studies to investigate how foam filling affects the acoustic radiation performance of circumferentially ribbed double-layer cylindrical shells. Their findings show that both ribbing and foam filling improve the sound insulation performance of the double-layer cylindrical shells.

The recent literature suggests that polyurethane foam has garnered significant attention in the field of acoustics owing to its superior vibration damping and noise reduction capabilities. However, the integration of porous materials in reinforced sandwich panels, though effective in minimizing structural vibration and lowering radiated sound pressure levels, increases the complexity of the mechanical and acoustic responses of composite sandwich panels. Currently, there is relatively limited research on the influence of polyurethane foam material parameters on the sound radiation performance of reinforced sandwich panel structures. Moreover, the sound radiation in the mid–low frequency range is closely related to many practical engineering and acoustic problems [15], and mid–low frequency noise not only severely affects the development of major strategic fields such as aerospace in China but also has an undeniable impact on the precision, service life, reliability, and safety of national defense equipment [16]. Therefore, this study employs a combined experimental and simulation approach to investigate the impact of foam parameters within the 1–2000 Hz mid–low frequency range on the sound radiation performance of foam-filled reinforced sandwich panels. This research aims to provide a robust theoretical foundation and experimental data for optimizing acoustic design and material selection.

2. Laboratory Test

2.1. Laboratory Test

According to the standard GB/T 16404-1996 [17], the experimental apparatus is adjusted to meet the basic requirements for sound intensity testing.

The instruments used for this sound intensity test are shown in Figure 1, and their parameters are listed in Table 1.

Table 1. List of sound intensity experimental instruments.

NO.	Name	Model Number	Technical Parameters
1	Multi-Channel Data Acquisition Module	SCM-V8-E	Voltage/ICP Channels: 8 Max. sampling frequency: 204.8 kHz Max. effective bandwidth: 92 kHz
2	Sound Intensity Sensor	INV9212	Sensitivity: 50 mV/Pa Frequency ranges: 50 Hz~6.3 kHz The dynamic range of sound intensity: 20~146 dB



Figure 1. Image of the apparatus used in the sound intensity experiment: (a) collector; (b) sound intensity sensor.

The standard process for testing sound intensity includes exposing the test sample to different operating or force excitation conditions, causing sound radiation. Next, a sound intensity probe consisting of two microphones is placed in fixed positions within the sound field or moved between different points distributed uniformly on a surface. Sound pressure is measured at these positions. The gathered data from the signal acquisition equipment are subsequently combined and analyzed by computational software to generate the sound intensity curve for the recorded positions.

To investigate the sound radiation performance of reinforced sandwich panels, a specimen of such a panel was constructed. Welding large areas on relatively thin panels can easily lead to bending deformation, which significantly affects the acoustic and vibration performance of the sandwich panel. Therefore, stainless steel plates are bonded to the C-shaped reinforcing ribs using adhesive bonding to ensure that the sandwich panel remains as flat as possible. This enables a more accurate study of sound radiation issues. High-strength acrylic structural adhesive is used as the metal adhesive in this case. The main part of the specimen is shown in Figure 2, and it can be observed from the figure that the prepared reinforced sandwich panel model has holes at the edges of the upper and lower panels for easy lifting and bolt fastening.



Figure 2. Specimen of a reinforced sandwich panel.

The thickness of both the upper and lower panels in the reinforced sandwich panel is 3 mm, with a panel spacing of 19 mm. The C-shaped reinforcing rib has a thickness of 2 mm, the reinforcement spacing is 27 mm, and the edge height is 10 mm. The panel main body measures 300 mm × 150 mm × 25 mm. Sound is emitted from the specimen when it is subjected to continuous uniform hammer impacts, and the sound pressure level is measured. Since the experimental research focuses on the panels, the discussion primarily concerns the sound pressure level that is perpendicular to the panel surface. Therefore, the

measurement points are aligned in parallel on a plane 500 mm above the surface of the panel [17], as shown in Figures 3 and 4.

As shown in Figure 5, point 17 has been chosen as the excitation point because it is in close proximity to the center of the panel and avoids nodal positions of low-order modal shapes. Furthermore, this point exhibits relatively substantial sound radiation.

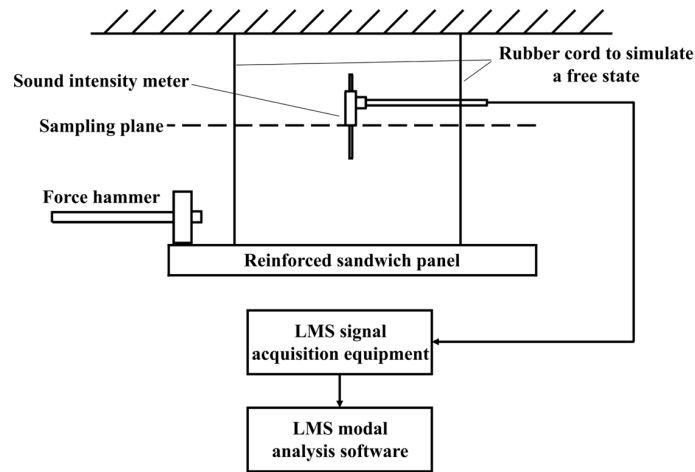


Figure 3. Schematic diagram of sound intensity experiment.



Figure 4. Layout diagram of sound intensity experiment site.

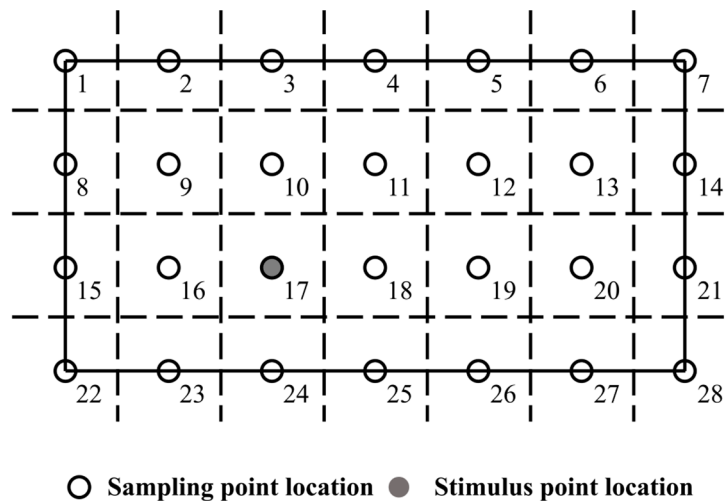


Figure 5. Schematic diagram of excitation point and sampling locations.

2.2. Experiments Conducted

For the sound intensity test experiment, a matched pair of microphones is used to construct a sound intensity probe in opposition. A spacer is positioned between the microphones to maintain a constant distance, enabling sound intensity calculations using the phase difference between the two microphones. Given the focus on the mid-to-low frequency range of sound radiation generated by the specimen, a spacer column of 12 mm is selected, corresponding to an allowable bandwidth range of 125–6300 Hz. The effective bandwidth ranges from 1 to 5120 Hz with an accuracy of 1 Hz. In order to ensure the precision and legitimacy of the results, a 10 s interval is allocated for the evaluation of each data point. Within each second, four data points are taken, starting from the measurement at time 0. A total of 41 measurements are taken in each sequence, and the final result is obtained by calculating the average result derived from these 41 data points.

According to the ISO9614-1 standard [18], valid measurements in general engineering applications occur when the sound pressure level measured exceeds the sound pressure level of background noise by 10 dB. Figure 6 displays the spectral graph of the radiated sound pressure level and the sound pressure level of background noise from the experimental results. It is discernible from Figure 6 that within the frequency range of around 1–200 Hz, the sound pressure level values measured experimentally are considerably akin to the ambient noise. This suggests that the ambient noise prevails within this frequency range. There are three main reasons for this: Firstly, the environment contains many sources of low-frequency noise, such as chassis cooling fans, which can penetrate effectively and are difficult to isolate completely. Secondly, hand-held sound intensity meters can experience slight vibrations during the measurement process, causing minor collisions between internal components and generating noise. Thirdly, the selectively absorbed high and mid-frequency sound waves increase the relative proportion of low-frequency sound due to reflections from surfaces such as the ground in the environment. In the 200–2000 Hz frequency range, most of the measured data, with the exception of a few troughs, exceeds the background noise sound pressure level by more than 10 dB, making the data obtained in this range credible and reliable. By measuring sound pressure and sound intensity at the sampling plane with the sound intensity meter and then using the radiated sound power formula, the radiated sound power within this area can be calculated directly, as shown in Figure 7.

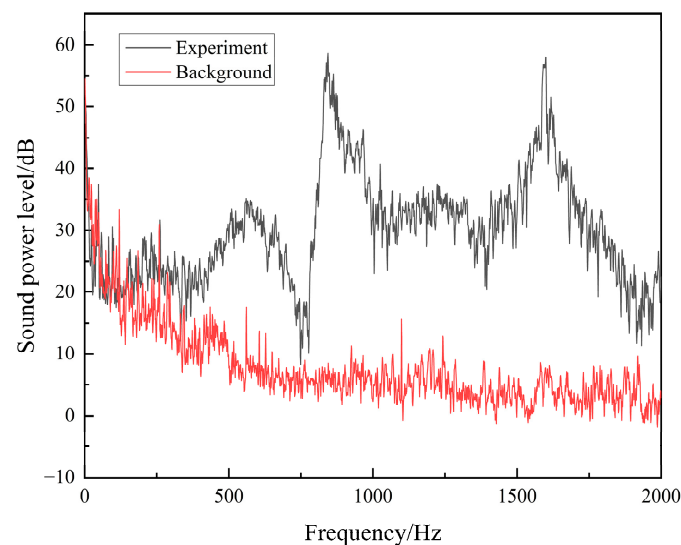


Figure 6. Comparison graph of sound radiation from the reinforced laminated panel and background sound pressure level.

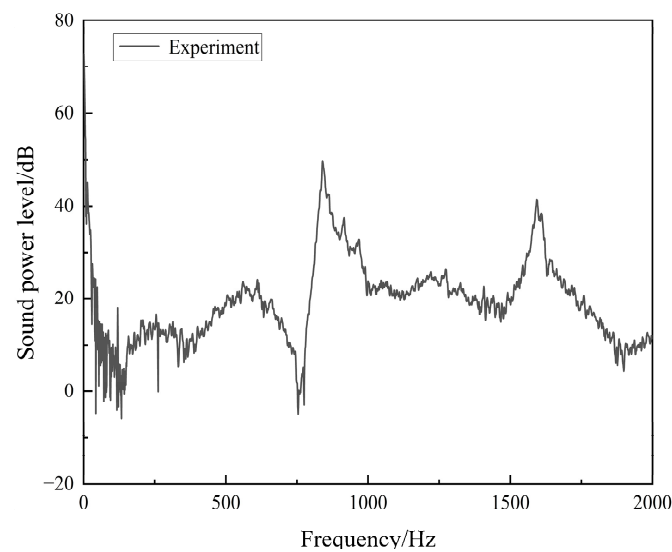


Figure 7. Frequency spectrum graph of radiated sound power level from the reinforced laminated panel.

3. Simulation Results and Experimental Verification

3.1. Simulation Modeling

To investigate the acoustic and vibration characteristics of the reinforced laminated panel, the reinforced laminated panel was modeled using SolidWorks 2021 3D modeling software. The constructed 3D model was imported as a STEP file into HyperMesh 2017 software for meshing, and the resulting 3D model and finite element model are shown in Figure 8.

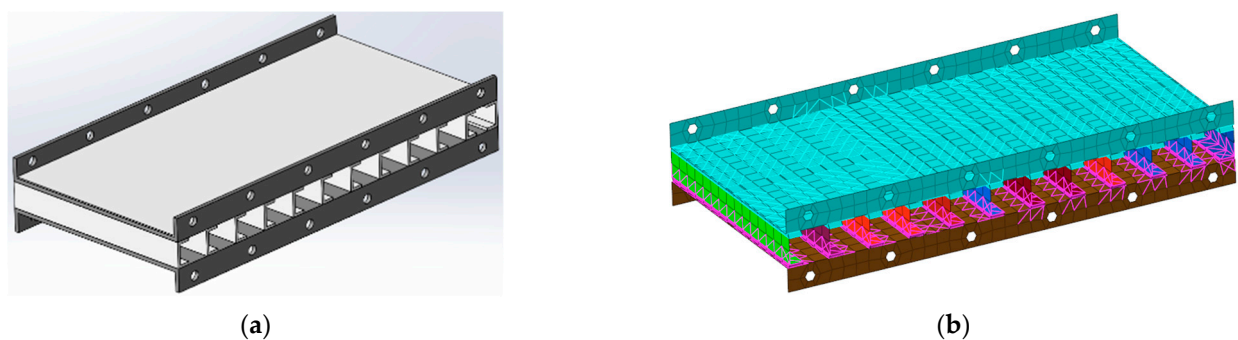


Figure 8. Finite element modeling: (a) 3D model; (b) finite element model.

As shown in the figure, both the top and bottom panels and the C-shaped ribs are discretized using QUAD square elements with a mesh size of 10 mm, for a total of 2070 elements. The connection between the C-shaped ribs and the upper and lower plates is made using RBE3 elements, for a total of 3432 elements. The finite element model of the reinforced laminated panel consists of 5502 structural elements. The material properties of stainless steel and acrylic structural adhesive are given in Table 2.

Table 2. Material properties of the reinforced laminated panel.

Material	Density (kg·m ³)	Young's Modulus (MPa)	Poisson's Ratio
Stainless	7700	210,000	0.30
Acrylic structural adhesive	900	5000	0.41

Import the established finite element model into the acoustic simulation software. Prior to acoustic preprocessing of the model, check the mass and quality of all nodes and

elements. Generate acoustic envelope surfaces. Set the material parameters and fluid properties for the respective structures. Simultaneously, establish coupling relationships between the structures and cavities. To simulate the experimental conditions, initially, utilize the force–time curve obtained from tapping the small plate with a small hammer. Convert it into a force–frequency curve using Fourier transform and import it into the software as a force excitation. Apply it to the corresponding structural mesh nodes for the experiment. To simulate the effect of ground reflection on the sound radiation, an automatic matching layer (AML) is applied to the fluid mesh surfaces outside the bottom surface of the lower cavity. The length of the lower cavity corresponds to the distance between the bottom surface of the panel and the ground during the experiment, approximately 700 mm. To simulate vibration behavior under free conditions, no constraints are applied. To be consistent with the experiment, 28 evenly distributed planar field point grids are placed approximately 500 mm above the panel for sampling. The total number of fluid elements is 27,005. The model is shown in Figure 9. Using the direct acoustic–structural coupling method, the frequency range for the solution is set between 1 and 2000 Hz, with a solution step of 1 Hz. The acoustic power at each node of the planar field point is computed and superimposed, followed by taking the average to obtain the overall acoustic power. Subsequently, the simulation results are compared against the experimental results.

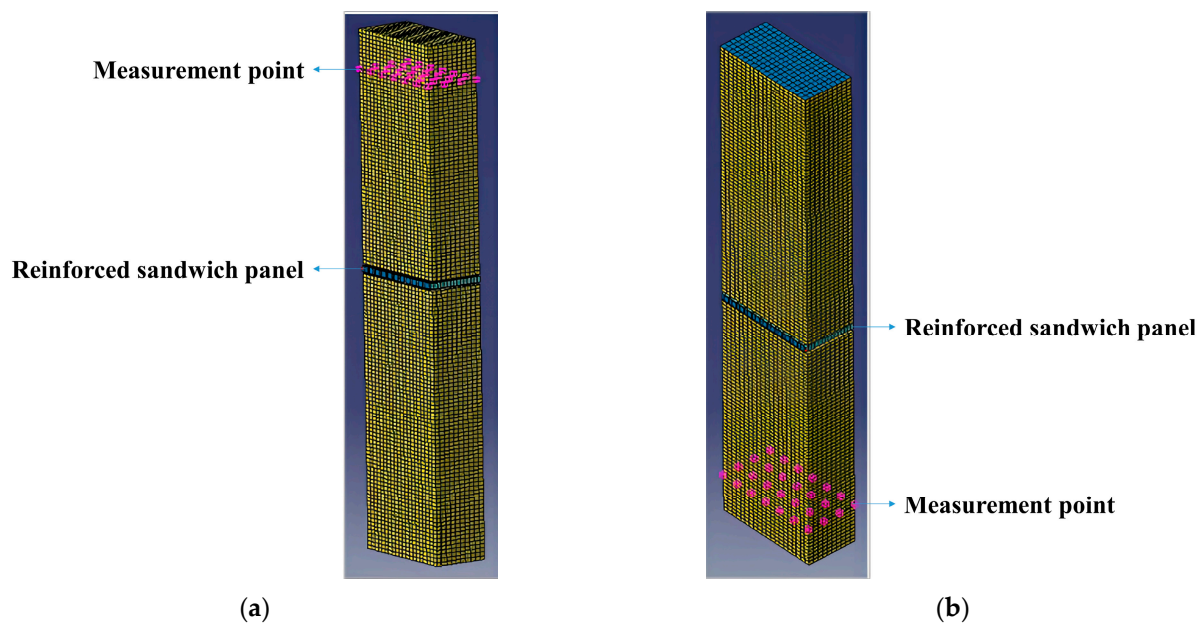


Figure 9. Acoustic finite element modeling of small plates: (a) top of the model; (b) underneath the model.

3.2. Validation of Simulation Models

The simulated sound power curve is compared with the experimentally measured sound power curve from Section 2.2 as shown in Figure 10. It can be seen from Figure 10 that the simulation results are in general agreement with the experimental results. The two main peak frequencies are at 855 Hz and 1589 Hz, with errors of approximately 1.79% and 0.25% compared to the experimental results, which is within a reasonable range. In different frequency ranges, the differences in sound power levels between the simulation and experiment are characterized by the simulation results having larger peaks, while being slightly lower at non-peak frequencies. This can be attributed to possible errors in the preparation process and the experimental environment of the sample, while the results of the simulation model are more idealized. The non-uniformity caused by manufacturing processes can lead to structural changes and increased internal damping in experiments. While this increases the dissipation of vibration energy and suppresses peaks, it can also cause noticeable vibrations at frequencies not predicted by theory, leading to sound

radiation. In conclusion, the finite element model developed in this study is reliable and accurate.

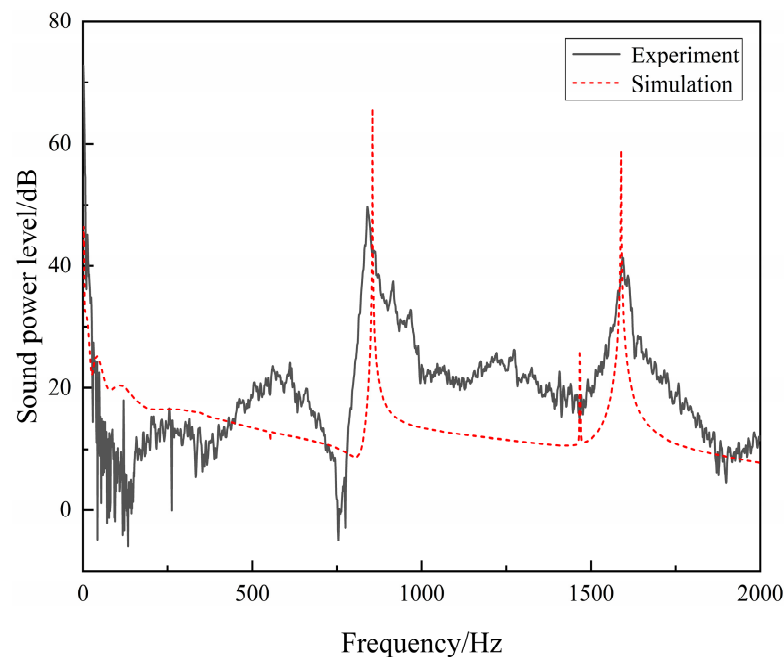


Figure 10. Comparison of experimental and simulated sound power level curves.

4. Simulation Study on Foam Acoustic Parameters

To investigate the influence of foam-filled panels on sound radiation performance in different directions, an AML layer is added to the floor part of the model set up in Section 3.2 to simulate an open environment. In addition, the air in the internal cavity is replaced with polyurethane foam. The simulation acoustic parameters of the polyurethane foam are set as shown in Table 3.

Table 3. Acoustic characterization parameters of polyurethane foam.

Static Flow Resistivity (Pa·s/m ²)	Porosity	Tortuosity Factor	Viscous Characteristic Length (mm)	Thermal Characteristic Length (mm)
87,000	0.97	2.52	0.037	0.119

The structure of porous materials is primarily composed of interlocking foam frameworks, forming a complex network. The internal pore structure mainly includes closed pores, semi-open pores, and open pores. Consequently, the propagation of sound inside porous materials is challenging to study at the microscale. Johnson, Allard, and others [19,20] proposed the use of five acoustic parameters, including porosity, static flow resistivity, tortuosity factor, viscous characteristic length, and thermal characteristic length, to describe the propagation of sound fields within porous materials. They established the equivalent fluid model known as the Johnson–Champoux–Allard model. Using the Johnson–Champoux–Allard porous material model, the filled polyurethane foam is treated as a special type of fluid medium, and the acoustic parameters of the material are entered into the simulation. The radiated sound power levels are measured at a plane 500 mm above the bottom surface to compare the effects of the different acoustic parameters of the foam on the sound radiation performance of the reinforced sandwich panel.

4.1. Effect of Foam Static Flow Resistivity on Acoustic Radiation Performance

The static flow resistivity of porous materials is a parameter that characterizes the magnitude of fluid flow resistance within porous materials. It may be determined by

dividing the pressure difference across the porous material by the volumetric velocity of fluid passing through the porous material, as demonstrated in Equation (1).

$$R = \frac{\Delta p}{vd}, \tag{1}$$

here Δp represents the pressure difference between the two sides of the porous medium, v denotes the air average flow velocity per unit area of the material, and d stands for the thickness of the sample.

Keeping other parameters constant, the static flow resistivity of the foam is set to its original value, 1.2 times the original value and 0.8 times the original value, which are 87,000 Pa·s/m², 104,400 Pa·s/m², and 69,600 Pa·s/m², respectively. These values are inserted into the calculations to obtain the radiated sound power at different static flow resistances, as shown in Figure 11.

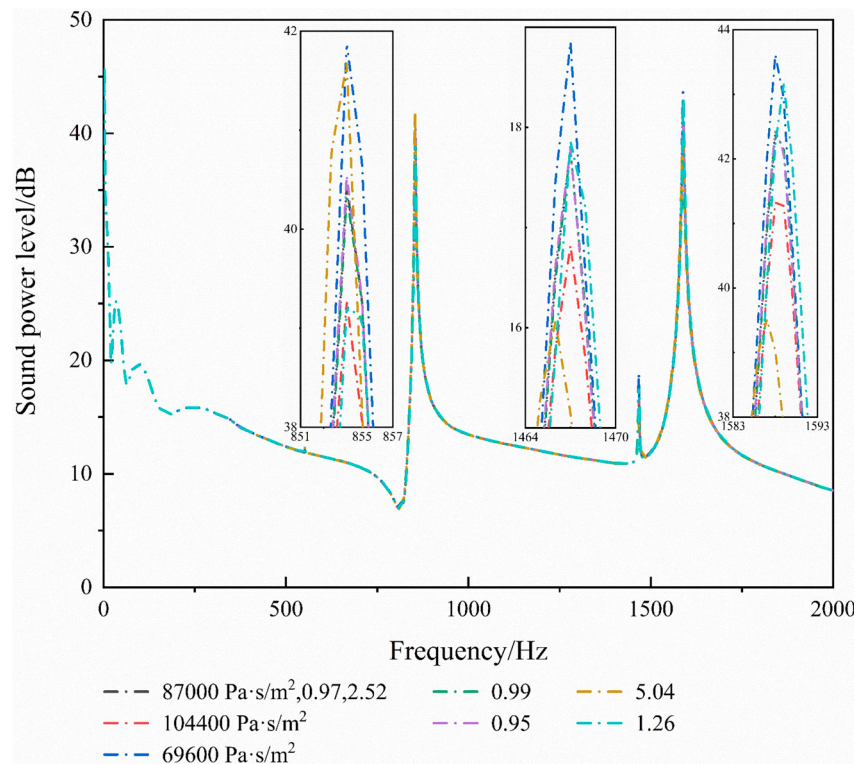


Figure 11. Comparative graph of radiated sound power level curves of foam-filled panels at various static flow resistivity, porosities, and tortuosity factors.

From Figure 11, it can be seen that as the static flow resistance of the foam increases, the radiated sound power gradually decreases. According to Table 4, at 854 Hz, the peak sound power levels corresponding to increasing static flow resistivity are 41.88 dB, 40.43 dB, and 39.27 dB, respectively. At 1467 Hz, they are 18.85 dB, 17.75 dB, and 16.82 dB and at 1588 Hz they are 43.61 dB, 42.41 dB, and 41.32 dB, respectively. This is because as the static flow resistance increases, so does the acoustic impedance during sound propagation.

Calculations show that as the static flow resistance of the foam increases, the effectiveness of the unit static flow resistance in suppressing radiated sound power gradually decreases. The reductions are 1.44 dB to 1.17 dB, 1.07 dB to 0.96 dB, and 1.19 dB to 1.10 dB, respectively, showing a non-linear relationship. Comparing the numerical values at different frequencies, it can be seen that the suppression effect of unit static flow resistance is significantly better at peak frequencies than at non-peak frequencies, and the suppression effect is more pronounced at larger peak frequencies than at smaller peak frequencies.

Table 4. Table of radiated sound power level results for foam-filled panels at various static flow resistivity, porosities, and tortuosity factors.

Parameter	Peak Frequency	Sound Power Level
87,000 Pa·s/m ²	854 Hz	41.88 dB
	1467 Hz	18.85 dB
	1588 Hz	43.61 dB
104,400 Pa·s/m ²	854 Hz	40.43 dB
	1467 Hz	17.75 dB
	1588 Hz	42.41 dB
69,600 Pa·s/m ²	854 Hz	39.27 dB
	1467 Hz	16.82 dB
	1588 Hz	41.32 dB
0.97	854 Hz	40.63 dB
	1467 Hz	17.80 dB
	1588 Hz	42.50 dB
0.99	854 Hz	40.73 dB
	1467 Hz	17.81 dB
	1588 Hz	42.53 dB
0.95	854 Hz	40.54 dB
	1467 Hz	17.79 dB
	1588 Hz	42.46 dB
2.52	854 Hz	39.22 dB
	1467 Hz	17.86 dB
	1588 Hz	43.17 dB
5.04	854 Hz	40.44 dB
	1467 Hz	17.78 dB
	1588 Hz	42.42 dB
1.26	854 Hz	41.68 dB
	1467 Hz	16.06 dB
	1588 Hz	39.51 dB

4.2. Effect of Foam Porosity on Acoustic Radiation Performance

Porosity is a parameter that characterizes the proportion of internal pore space within porous materials, as shown in Equation (2) [21]. Porosity not only affects the acoustic radiation performance of foam materials but increasing the porosity of foam materials can also reduce their thermal conductivity, thereby improving their thermal insulation performance [22].

$$\phi = \frac{V_a}{V_t} = 1 - \frac{V_m}{V_t}, \tag{2}$$

here ϕ signifies the porosity of the porous material, V_a denotes the air volume within the porous material, V_t stands for the total volume of the porous material, and V_m represents the volume of the porous material’s framework.

Keeping all other parameters constant, the foam porosity is set to 0.99, 0.97 (the original value), 0.95, 0.93, and 0.91. The radiated power at various porosities is calculated, and Figure 11 displays the results.

According to Table 4, at 854 Hz, the sound power levels increase from low to high porosities at 40.73 dB, 40.63 dB, 40.54 dB, 40.44 dB, and 40.35 dB. Correspondingly, at 1467 Hz, the levels at low to high porosities are 17.81 dB, 17.80 dB, 17.79 dB, 17.78 dB, and 17.77 dB. Similarly, at 1588 Hz, the levels at low to high porosities are 42.53 dB, 42.50 dB, 42.46 dB, 42.42 dB, and 42.38 dB. Calculations based on the above data show that a 1% increase in porosity at 854 Hz, 1467 Hz, and 1588 Hz leads to a decrease in radiated sound power levels by 0.0475 dB, 0.005 dB, and 0.01875 dB, respectively. It is clear that altering the porosity alone has a negligible impact on the sound-radiating performance and can be disregarded.

In conclusion, an increase in porosity results in a gradual decrease in radiated sound power at various peak points. Nonetheless, within an acceptable range and without accounting for density changes attributable to porosity fluctuations, the impact of porosity on the radiated sound power is relatively insignificant.

4.3. Effect of Foam Tortuosity Factor on Acoustic Radiation Performance

The tortuosity factor is a parameter that quantifies the degree of curvature of internal cavities in porous materials. Its essence is the ratio of the shortest path between one end and the other end of the porous material to the material's thickness. Therefore, it is a dimensionless number with a minimum value of 1 and no theoretical upper limit [23]. To examine how the tortuosity factor of the filled foam affects the reinforced laminated plate's structural sound radiation performance, other parameters were kept constant as different foam tortuosity factor values were tested: the original value, double the original value, and half the original value, which equate to 2.52, 5.04, and 1.26, respectively. Using the provided values in the calculations, Figure 11 illustrates the sound radiation power for different tortuosity factors.

According to Table 4, at frequencies near 854 Hz, the values are 39.22 dB, 40.44 dB, and 41.68 dB. At frequencies near 1467 Hz, the values are 17.86 dB, 17.78 dB, and 16.06 dB. Finally, at frequencies near 1588 Hz, the corresponding values are 43.17 dB, 42.42 dB, and 39.51 dB. This suggests that, within the mid–low frequency range, there is a positive correlation between the tortuosity factor and the radiated sound power. As the frequency increases, the tortuosity factor increasingly inhibits the radiated sound power, with the magnitude of this effect rising with the tortuosity factor.

In conclusion, it can be seen that different peak frequencies exhibit varying effects on the sound radiation of the plate with respect to the tortuosity factor. At approximately 854 Hz, the radiated sound power increases as the tortuosity factor increases. However, around 1467 Hz and 1588 Hz, the radiated sound power decreases as the tortuosity factor increases. In addition, it should be noted that at any peak frequency, an increase in the tortuosity factor results in a shift of the sound power peak towards lower frequencies.

4.4. Effect of Foam Viscous Characteristic Length on Acoustic Radiation Performance

The viscous characteristic length Λ is a parameter that characterizes the energy loss due to the viscosity of the fluid inside porous materials. It can be defined as follows:

$$\Lambda = 2 \frac{\int_V v_i^2(r) dV}{\int_A v_i^2(r_w) dA'} \quad (3)$$

here $v_i(r)$ represents the velocity of the non-viscous fluid within the pore, $v_i(r_w)$ stands for the velocity of the fluid at the interface between the pore and the material skeleton, A represents the pore surface area, and V denotes the volume of the pore.

Keeping all other parameters unchanged, the foam's viscous characteristic length was, respectively, assigned to its original value, twice the original value, and half the original value, that is, 0.037 mm, 0.074 mm, and 0.0185 mm. The sound radiation power was then calculated at different viscous characteristic lengths, as depicted in Figure 12.

According to Table 5, at approximately 854 Hz, the sound powers increase from small to large viscous characteristic lengths as follows: 41.26 dB, 40.44 dB, and 39.83 dB. The corresponding sound powers around 1467 Hz are 16.15 dB, 17.78 dB, and 18.01 dB, while near 1588 Hz the corresponding sound powers are 40.00 dB, 42.42 dB, and 42.89 dB. Calculation demonstrates that, at approximately 854 Hz, there are consecutive reductions of 0.82 dB and 0.61 dB, suggesting a gradual decline in sound radiation suppression per unit viscous characteristic length. Technical abbreviations are defined on their first use. In contrast, at around 1467 Hz, the sound radiation power increases consecutively by 1.63 dB and 0.23 dB; and at about 1588 Hz, the sound radiation power rises by 2.42 dB and

0.47 dB, respectively. This suggests that the rise in the length of the viscous feature has minimal effect on the improvement of sound radiation at higher frequencies.

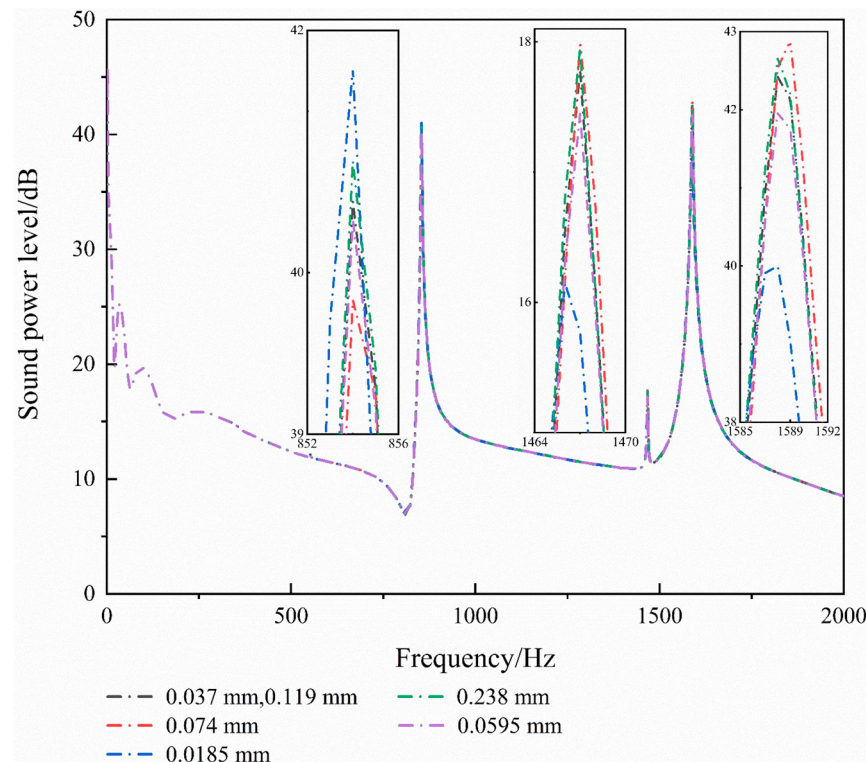


Figure 12. Comparative graph of radiated sound power level curves of foam-filled panels at various viscous characteristic lengths and thermal characteristic lengths.

Table 5. Table of radiated sound power level results for foam-filled panels at varying viscous characteristic lengths and thermal characteristic lengths.

Parameter	Peak Frequency	Sound Power Level
0.037 mm	854 Hz	41.26 dB
	1467 Hz	16.15 dB
	1588 Hz	40.00 dB
0.074 mm	854 Hz	40.44 dB
	1467 Hz	17.78 dB
	1588 Hz	42.42 dB
0.0185 mm	854 Hz	39.83 dB
	1467 Hz	18.01 dB
	1588 Hz	42.89 dB
0.119 mm	854 Hz	40.33 dB
	1467 Hz	17.45 dB
	1588 Hz	41.96 dB
0.238 mm	854 Hz	40.45 dB
	1467 Hz	17.75 dB
	1588 Hz	42.43 dB
0.0595 mm	854 Hz	40.69 dB
	1467 Hz	17.95 dB
	1588 Hz	42.67 dB

In conclusion, when the thermal characteristic length is kept constant, the impact of the viscous characteristic length on the radiated sound power varies at different frequencies. Additionally, the viscous characteristic length solely has a notable impact at peak

frequencies. Around 854 Hz, the radiated sound power decreases continuously as the viscous characteristic length increases, while around 1467 Hz and 1588 Hz, the radiated sound power increases with an increase in the viscous characteristic length.

4.5. Effect of Foam Thermal Characteristic Length on Acoustic Radiation Performance

The thermal characteristic length is a key parameter that defines the microstructure of porous materials and their ability to exchange heat internally with fluids. Its physical essence is the mean pore radius in porous materials, with a unit of mm. Its standard value is generally approximately double the viscous characteristic length of the identical material. In order to investigate the influence of the thermal characteristic length of foam filled on the acoustic radiation performance of the reinforced sandwich panel structure, while keeping other parameters unchanged, the foam thermal characteristic length is set to its original value, twice the original value, and half the original value, namely, 0.119 mm, 0.238 mm, and 0.0595 mm. By inserting these values into the equation, the acoustic radiation power can be determined for various thermal characteristic lengths, as illustrated in Figure 12.

According to Table 5, at 854 Hz, the sound power corresponding to a decreasing thermal characteristic length is 40.33 dB, 40.45 dB, and 40.69 dB, respectively. At 1467 Hz, the sound power corresponding to a decreasing thermal characteristic length is 17.45 dB, 17.75 dB, and 17.95 dB, respectively. Lastly, at 1588 Hz, the sound power corresponding to a decreasing thermal characteristic length is 41.96 dB, 42.43 dB, and 42.67 dB, respectively. It can be deduced that at 854 Hz, the sound power level attenuation is roughly proportional to the decrease in thermal characteristic length. However, for the last two peak frequencies, there is a clear occurrence that the suppression effect on sound power radiation is stronger with a smaller thermal characteristic length. This is because the foam structure can more efficiently convert high-frequency sound waves into thermal energy, and heat exchange efficiency is vital for suppressing sound radiation in the higher frequency range. Therefore, selecting fine foam materials, under the same porosity, is advantageous for reducing the sound radiation of the reinforced sandwich panel.

In conclusion, it is apparent that alterations in thermal characteristic length do not markedly impact the peak frequencies of the curves. Additionally, there is a uniform growth in sound radiation power for all peak frequencies with an increase in thermal characteristic length. This arises from the circumstance that, under constant volume and porosity, the doubling of the size of individual pores leads to a halving of the total heat exchange area.

5. Conclusions

This study uses an experimental- and simulation-based approach to examine the influence of foam acoustic parameters on the sound radiation capability of reinforced sandwich panels filled with foam within the 1–2000 Hz frequency range. The following findings are reported:

1. Without taking into account structural effects, modifying the acoustic parameters of foam has a minor influence on the peak frequency of radiated sound power, as well as the sound radiation performance in non-peak frequency ranges of the sandwich panel. Nevertheless, it has a significant impact on the peak radiated sound power.
2. Within a reasonable range of foam parameter values, the porosity has a minimal impact on sound radiation performance; hence, it can be practically ignored. Peak sound radiation performance is significantly affected by static flow resistivity and tortuosity factors. A 20% variance in static flow resistivity and a 100% variance in tortuosity factor resulted in a decrease of 1.44 dB and 2.91 dB, respectively, in the peak radiated sound power level at specific frequencies. Technical term abbreviations such as “static flow resistivity” and “tortuosity factor” will be explained upon first use.
3. Among the other foam parameters, reducing the thermal characteristic length and raising static flow resistivity both improve the plate’s sound radiation performance. Nevertheless, the effects of the tortuosity factor and viscous characteristic length

on the sound radiation vary depending on the frequency. Specifically, within the 1–1000 Hz frequency range, reducing the tortuosity factor and lengthening the viscous characteristic both enhance the plate's sound radiation efficiency. In contrast, within the 1000–2000 Hz frequency range, the converse trend is apparent.

This study has practical applications in real-life contexts. For example, in residential, commercial, and industrial construction domains, our research findings provide guidance to architects and engineers on how to optimize sandwich panel materials to achieve superior sound insulation. This creates a calmer indoor environment [24]. In the field of aerospace engineering, aircraft manufacturers can achieve effective noise reduction for passengers during flights by adjusting the foam parameters in sandwich panels. This results in a more comfortable flying experience. These application cases demonstrate the practical application of our research, offering guidance across a range of domains. They highlight the importance of our research in improving environmental quality, enhancing product performance, and providing superior user experiences [25,26].

Author Contributions: B.L., proposed the ideas, steps, and details of the experiment, most of the experiments were completed by N.W., H.D., Z.Z., W.K. and L.W., where N.W. was instrumental in the proper conduct of the experiments and wrote the article together with B.L., and all the authors analyzed the data and discussed the conclusions. All authors have read and agreed to the published version of the manuscript.

Funding: The work is supported by the 2022 Knowledge Innovation Dawn Special Plan Project (2022010801020393), Research and Innovation Initiatives of WHPU (2022J04), Natural Science Foundation of Hubei Province (2021CFB292). This work was finished at Wuhan Polytechnic University, Wuhan.

Institutional Review Board Statement: Not applicable for studies not involving humans or animals.

Informed Consent Statement: Not applicable for studies not involving humans or animals.

Data Availability Statement: No new data are created.

Conflicts of Interest: The authors declare no conflict of interest.

References

1. Tang, Z.M. Status of noise pollution, hazards and their management. *Ecol. Econ.* **2017**, *33*, 6–9.
2. Xia, Q.Q.; Chen, Z.J. Vibro-acoustic characteristics of ring stiffened cylindrical shells using structure reactance improvement. *J. Huazhong Univ. Sci. Tech. (Nat. Sci. Ed.)* **2012**, *40*, 90–94.
3. Tang, W.L.; He, B.R. Approximate analytic solution of vibration and sound radiation from stiffened finite cylindrical shells in water. *Acta Acust.* **2001**, *26*, 1–5.
4. Birman, V.; Kardomateas, G.A. Review of current trends in research and applications of sandwich structures. *Compos. Part B Eng.* **2018**, *142*, 221–240. [[CrossRef](#)]
5. Bahrami-Novin, N.; Shaban, M.; Mazaheri, H. Flexural response of fiber-metal laminate face-sheet/corrugated core sandwich beams. *J. Braz. Soc. Mech. Sci. Eng.* **2022**, *44*, 183. [[CrossRef](#)]
6. Wan, Z.; Liu, Y.; Chen, X.; Wu, H.; Yin, F.; Gao, R.; Li, Y.; Zhao, T. Experimental and Numerical Investigations of the Vibration and Acoustic Properties of Corrugated Sandwich Composite Panels. *Appl. Sci.* **2022**, *12*, 8553. [[CrossRef](#)]
7. Sahib, M.M.; Kovács, G. Elaboration of a Multi-Objective Optimization Method for High-Speed Train Floors Using Composite Sandwich Structures. *Appl. Sci.* **2023**, *13*, 3876. [[CrossRef](#)]
8. Li, Q.; Yang, D. Mechanical and Acoustic Performance of Sandwich Panels with Hybrid Cellular Cores. *J. Vib. Acoust.* **2018**, *140*, 061016.
9. Thamburaj, P.; Sun, J.Q. Optimization of Anisotropic Sandwich Beams for Higher Sound Transmission Loss. *J. Sound Vib.* **2002**, *254*, 23–36. [[CrossRef](#)]
10. Wang, L. Sound Radiation Responses and Acoustic Behavior of Sandwich Panel. Master's Thesis, The University of Regina, Regina, SK, Canada, 2019.
11. Arunkumar, M.P.; Pitchaimani, J.; Gangadharan, K.V.; Leninbabu, M.C. Vibro-acoustic response and sound transmission loss characteristics of truss core sandwich panel filled with foam. *Aerosp. Sci. Technol.* **2018**, *78*, 1–11. [[CrossRef](#)]
12. Khan, T.; Acar, V.; Aydin, M.; Hülagü, B.; Akbulut, H.; Seydibeyoğlu, M. A review on recent advances in sandwich structures based on polyurethane foam cores. *Polym. Compos.* **2020**, *41*, 2355–2400. [[CrossRef](#)]
13. Li, H.; Ren, X.H.; Yu, C.S.; Xiong, J.; Wang, X.P.; Zhao, J. Investigation of vibro-acoustic characteristics of FRP plates with porous foam core. *Int. J. Mech. Sci.* **2021**, *209*, 106697. [[CrossRef](#)]

14. Zheng, Z.Q.; Li, B.; Yan, S.L.; Qi, M.H.; Wang, N.; Kuang, W.J.; Wen, J.; Ma, Y. Acoustic radiation performance investigation of a double-walled cylindrical shell equipped with annular plates and porous foam media. *J. Low Freq. Noise Vib. Act. Control* **2023**, *42*, 851–865. [[CrossRef](#)]
15. Junger, M.C.; Feit, D. *Sound, Structures, and Their Interaction*; The MIT Press: Cambridge, MA, USA, 1972.
16. Chen, X. Noise Reduction inside Launch Vehicle Fairing Using Melamine Foam and Helmholtz Resonator. Ph.D. Thesis, Beijing Institute of Technology, Beijing, China, 2017.
17. GB/T 16404-1996; Acoustics—Determination of Sound Power Levels of Noise Sources Using Sound Intensity—Part 1: Measurement at Discrete Points. State Administration for Market Regulation: Beijing, China, 1996; p. 24.
18. ISO 9614-1-1993; Acoustics—Determination of Sound Power Levels of Noise Sources Using Sound Intensity—Part 1: Measurement at Discrete Points. ISO: Geneva, Switzerland, 1993.
19. Johnson, D.L.; Koplik, J.; Dashen, R.F. Theory of dynamic permeability and tortuosity in fluid-saturated porous media. *J. Fluid Mech.* **1987**, *176*, 379–402. [[CrossRef](#)]
20. Champoux, Y.; Allard, J.F. Dynamic tortuosity and bulk modulus in air-saturated porous media. *J. Appl. Phys.* **1991**, *70*, 1975–1979. [[CrossRef](#)]
21. Allard, J.F.; Atalla, N. *Propagation of Sound in Porous Media: Modelling Sound Absorbing Materials*, 2nd ed.; Wiley-Blackwell: Hoboken, NJ, USA, 2009.
22. Mort, R.; Vorst, K.L.; Curtzwiler, G.W.; Jiang, S. Biobased foams for thermal insulation: Material selection, processing, modelling, and performance. *RSC Adv.* **2021**, *11*, 4375–4394. [[CrossRef](#)] [[PubMed](#)]
23. Xin, F.; Wang, F.; Li, S. Qualitative relationship between the curvature factor and the microstructure of porous media. *J. Chem. Ind. Eng.* **2000**, *51*, 457–461.
24. Pott Pollenske, M. Limits and challenges of aircraft retrofitting for noise reduction. *CEAS Aeronaut. J.* **2019**, *10*, 69–76. [[CrossRef](#)]
25. Garg, N.; Gautam, C.; Devi, A. Airborne Sound Insulation of Sandwich Partition Panels and Masonry Constructions for Noise Control. *MAPAN* **2023**, *38*, 729–743. [[CrossRef](#)]
26. Erofejev, V.; Monich, D. Sound insulation properties of sandwich panels. *IOP Conf. Ser. Mater. Sci. Eng.* **2020**, *896*, 012005. [[CrossRef](#)]

Disclaimer/Publisher’s Note: The statements, opinions and data contained in all publications are solely those of the individual author(s) and contributor(s) and not of MDPI and/or the editor(s). MDPI and/or the editor(s) disclaim responsibility for any injury to people or property resulting from any ideas, methods, instructions or products referred to in the content.